第 41 卷 第 4 期：1167-1177 高电压技术 Vol.41, No.4: 1167-1177
2015 年 4 月 30 日 High Voltage Engineering April 30, 2015
DOI: 10.13336/j.1003-6520.hve.2015.04.014

Space Charge Behaviours in Polyethylene Under Combined AC and DC Electric Fields

C. Zhou, G. Chen
(The Tony Davies High Voltage Laboratory, University of Southampton, Southampton SO17 1BJ, United Kingdom)

Abstract：Polyethylene is one of the widely studied polymeric insulation materials, which have been used extensively for cable insulation. One of the major issues related to polymeric materials is its easy formation of space charge, a high chance to cause electric field distortions. This phenomenon is more significant under high voltage direct current (HVDC) stresses. Space charge can also be observed under high voltage alternative current (HVAC)stresses but with much less intensity due to the limited charge injection period and the effect of charge recombination caused by the constantly variance of the external fields. When considering the situation of an AC voltage combined with a DC offset, a possible scenario in HVDC technology, there was little research on charge dynamics in the insulation in terms of both experimental and simulation work. In this paper, a numerical simulation based a bipolar charge injection/transport model is used to obtain characteristics of space charge in polyethylene under the combined AC and DC high voltage at room temperature. The bipolar charge injection/transport model, which is widely used in HVDC space charge simulation, is applied in the combined conditions. The overall applied voltage, consisted of root mean square (RMS) values of the AC voltage and DC voltage, is kept the same, while the DC component's voltage ratio and AC component's frequency are changed respectively, to illustrate their effects on the space charge dynamics within the insulation under combined electric fields. The simulated charge distributions present notable differences when DC offset is increasingly added in, while relatively small differences when AC component's frequency altering, especially for the cases whose frequency exceeding 0.5 Hz.

Key words：space charge; bipolar charge transportation model; polyethylene; HVDC technology; cable insulation

0 Introduction

Over the years, space charge accumulation has been regarded as an important factor causing electrical failures of high voltage DC insulation. The presence of charge in the localised energy states of an insulator leads distortion in the internal fields. This distortion could be exacerbated by the presence of mechanical and thermal stresses existed from either the applied electric field or the local environment. Over the last few decades, several non-destructive charge mapping methods have been established to investigate the formation, transport, and neutralization of space charge within polymeric materials [1-2]. They provided inspiring understanding on charge injection, transport, trapping, detrapping and recombination within insulation materials. Besides, considerable efforts have been made to study space charge characteristics in polymeric insulation under DC conditions[3-5]. However, space charge behaviour under AC voltages and combined conditions, which are commonly situations in high voltage convertor transformers, has not been fully investigated. This paper mainly focuses on numerical modelling of space charge under combined AC and DC high voltage conditions. Polyethylene, especially low density type (LDPE), is chosen as the research material in order to simplify the simulated conditions and minimise influence factors.

Two possible reasons are accounted for the current limited research on space charge under complex electric stresses. Firstly, previous experimental measurements showed small amount of space charge can be observed under AC electric fields, and the accumulated amount of charge in the material was significantly reduced under high frequency conditions[6-7]. Therefore, space charge under complex electric stresses is assumed to be less harmful than that under a DC field and attracts much less attention. Secondly, the detection of space charge under complex stresses is relatively difficult comparing with meas-

urement under DC fields. Additionally, new proaches are required to deal with large amount of data analysis and phase identification.

Numerical modelling provides an alternative method to investigate charge dynamics within solid insulation. A bipolar charge transport model involving bipolar charge injection, transport, trapping, and recombination has been established to analyse the dynamics of space charge within solid dielectrics under DC high electric fields[8-9].It has been revealed that the simulation can represent both reasonable amount of charges and evolution of space charge in the transient process as well as the effect of long term stressing[10]. In this paper, the model is further developed to facilitate the simulation of space charge within polyethylene under combined AC and DC fields. Two factors of the applied fields, the percentage of the AC and DC voltage portion and frequency of the AC component, have been investigated. The simulated results are presented and analysed.

1 Bipolar Charge Transport Model

Based on observed charge in experiments, the bipolar charge transport model assumes that opposite charges contribute to charge injection, transport, and trapping in the bulk of insulators as well as recombination process, when subjected to electric fields[3]. The model has been implemented to simulate space charge within LDPE films which have been subdivided into small elements and the carrier fluxes between elements for the simulation in the present paper, as shown in Fig.1. An unbalanced partition is chosen in the computing process, in consideration of the charges primarily accumulated in the region close to the interface when the applied field constantly alters its polarity[11].

All the charges are assumed to be sourced from the Schottky injection from the boundaries, as Equation (1) shows

$$\begin{cases} J_{\mathrm{e}}(0,t) = AT^2 \exp(\dfrac{-ew_{\mathrm{ei}}}{kT}) \exp(\dfrac{e}{kT}\sqrt{\dfrac{eE(0,t)}{4\pi\varepsilon}}) \\ J_{\mathrm{h}}(d,t) = AT^2 \exp(\dfrac{-ew_{\mathrm{hi}}}{kT}) \exp(\dfrac{e}{kT}\sqrt{\dfrac{eE(d,t)}{4\pi\varepsilon}}) \end{cases} \tag{1}$$

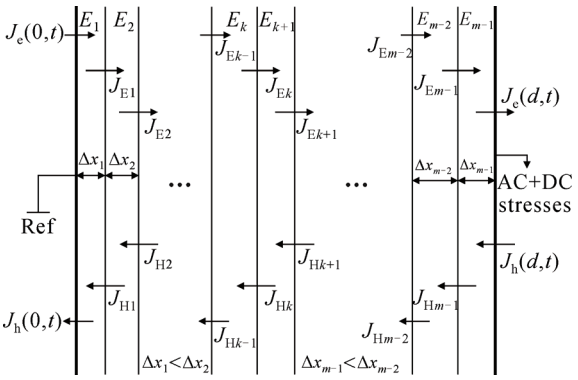

Fig.1 Discretization of modelled sample under combined AC and DC stress

where, $J_{\mathrm{e}}(0, t)$ and $J_{\mathrm{h}}(d, t)$ are the injected current density of the electrons at the cathode and of the holes at the anode respectively; $E(0, t)$ and $E(d, t)$ are the electric fields accordingly; A is the Richardson constant, normally 1.20×10^{6} $\mathrm{A\cdot m^{-2}\cdot K^{-2}}$; T is the absolute temperature; e is the elementary charge; k is the Boltzmann constant, 1.38×10^{-23} $\mathrm{m^2\cdot kg\cdot s^{-2}\cdot K^{-1}}$; w_{ei} and w_{hi} are the injection barrier heights for electrons and holes respectively; and ε is the permittivity of the dielectric. While the extraction of charge from the electrodes can be calculated using Equation (2) as below

$$\begin{cases} J_{\mathrm{e}}(d,t) = \mu_{\mathrm{e}} E(d,t) n_{\mathrm{e\mu}}(d,t) \\ J_{\mathrm{h}}(0,t) = \mu_{\mathrm{h}} E(0,t) n_{\mathrm{h\mu}}(0,t) \end{cases} \tag{2}$$

where $J_{\mathrm{e}}(d, t)$ and $J_{\mathrm{h}}(0, t)$ are the extracted fluxes of electrons and holes from the electrodes; μ_{e} and μ_{h} are the mobilities of charge carriers and $n_{\mathrm{e\mu}}$ and $n_{\mathrm{h\mu}}$ are the density of mobile electrons and holes respectively.

The charge transport is described by the conduction process characterised using the mobility of the charge carriers. Mobility of the electrons and holes are computed differently in consideration of their different field dependences[12]. The mobility of electrons is analysed using the power's law[13] while for holes the mobility is represented utilising a curve-fitting function of Fig.2(a)[14]. The specific process is illustrated below:

$$J = \mu n E = \nu n$$

$$\nu = \mu_0 E^{m_1}$$

$$v=\begin{cases} a_1E+a_2E^2+a_3E^3, & 0\le E\le E_c \\ bE^{-m_2}, & E>E_c \end{cases} \quad \text{(Holes)} \tag{3}$$

Where J is the conduction current density; μ is the field dependent mobility of charge carrier; v is the drift velocity; μ_0 is the mobility under low electric fields; m_1, m_2 are the power indexes; n is the density of mobile species; and E is the local electric field; a_1, a_2, a_3, b are the constants obtained from curve-fitting; E_c is a critical field separating the low and high electric field phenomena for positive charge carriers; in Fig.2 (a), it is 100 MV/m.

When charges move within the bulk they can be captured by the trap centres originating from physical and chemical defects. We assume that the polymer only contains two types of traps, shallow traps and deep traps. And charges in shallow traps are able to detrap, becoming movable, while those in deep traps cannot.

Theoretically, charge carriers within solids are governed by three basic equations, namely the Poisson's equation (Equation (4)), transport equation (Equation (5)) and continuity equation (Equation (6)), describing the charge density, current density and electric fields as a function of time and spatial position.

$$\frac{\partial E(x,t)}{\partial x}=\frac{\rho(x,t)}{\varepsilon} \tag{4}$$

$$J(x,t)=\mu n(x,t)E(x,t) \tag{5}$$

$$\frac{\partial n(x,t)}{\partial t}+\frac{\partial J(x,t)}{\partial x}=s \tag{6}$$

where ρ is the net charge density; ε is the permittivity of the dielectric; and s is the source term.

The continuity equation can be split into two, Equation (7) and Equation (8). Equation (7) is only controlled by the conduction current density, while Equation (8) is using the contribution of source term S to update the charge density in the previous one.

$$\frac{\partial n(x,t)}{\partial t}+\frac{\partial J(x,t)}{\partial x}=0 \tag{7}$$

$$\frac{\partial n(x,t)}{\partial t}=s \tag{8}$$

The source term, s is designed to present the effects of charge recombination and trapping phenolmena, and in consideration of each species (mobile/trapped electrons/holes) Equation (8) should be presented in four terms

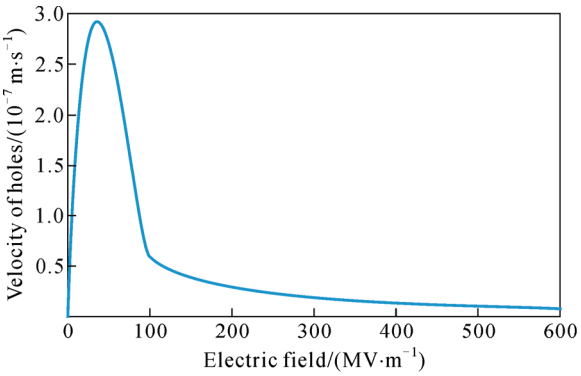

(a) Measured results of Chen

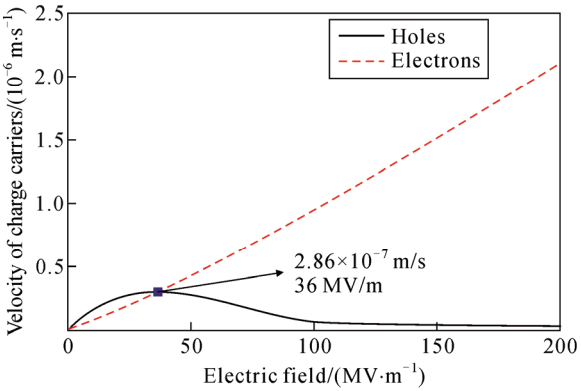

(b) Used velocities of holes and electrons in the simulation

Fig.2 Measured holes' velocity versus fields and used velocities versus fields

$$\begin{cases} s_1=\dfrac{\partial n_{e\mu}}{\partial t}=-S_1n_{ht}n_{e\mu}-S_2n_{h\mu}n_{e\mu}-B_en_{e\mu}\left(1-\dfrac{n_{et}}{n_{0et}}\right) \\ s_2=\dfrac{\partial n_{h\mu}}{\partial t}=-S_2n_{et}n_{h\mu}-S_3n_{h\mu}n_{e\mu}-B_hn_{h\mu}\left(1-\dfrac{n_{ht}}{n_{0ht}}\right) \\ s_3=\dfrac{\partial n_{et}}{\partial t}=-S_2n_{h\mu}n_{et}-S_0n_{ht}n_{et}+B_en_{e\mu}\left(1-\dfrac{n_{et}}{n_{0et}}\right) \\ s_4=\dfrac{\partial n_{ht}}{\partial t}=-S_1n_{ht}n_{e\mu}-S_0n_{ht}n_{et}+B_hn_{h\mu}\left(1-\dfrac{n_{ht}}{n_{0ht}}\right) \end{cases} \tag{9}$$

Where s_1, s_2, s_3, s_4 are the source terms for each species; S_0, S_1, S_2, S_3 are the recombination coefficients; B_e and B_h are the trapping coefficients for electrons/holes; $n_{e\mu}$, n_{et}, $n_{h\mu}$, n_{ht} respectively indicate the densities of each species: mobile electrons, trapped electrons, mobile holes and trapped holes; n_{0et}, n_{0ht} are indicating the trap densities for electrons and holes. The detailed meaning of these parameters is illustrated below in Fig.3.

The recombination of opposite species can be represented by the total recombination rate T_R as

shown in Equation (10).

$$T_R = S_0 n_{ht} n_{et} + S_1 n_{ht} n_{e\mu} + S_2 n_{et} n_{h\mu} + S_3 n_{h\mu} n_{e\mu} \quad (10)$$

The total current density $J_t(x,t)$ can be computed using Equation (11) and the first term is the conduction current density and second is the displacement current density.

$$J_t(x,t) = J(x,t) + \varepsilon \frac{\partial E(x,t)}{\partial t} \quad (11)$$

The applied voltage used in the simulation can be expressed as

$$U = U_p \sin(2\pi f t) + U_{DC} \quad (12)$$

where, U_p is the peak voltage; f is the frequency of AC voltage; U_{DC} is the DC voltage component.

Different parameter settings have been used for electrons and holes respectively for this simulation. The injection barrier for holes is set lower than the electrons in order to demonstrate the phenomenon that holes are easier to be injected into the insulation, comparing with electrons[15]. All the parameter values are chosen in accordance with those used under pure AC and DC conditions[11,15]. Specific parameters are listed in Table 1.

These settings of the parameters will generate packet-like charge distribution curves under relatively high DC electric fields[15].

2 Simulation Results

In this section in order to describe the percentage of DC component U_{DC} within the combined electric stress, a DC offset ratio is defined as

$$R_{DCO} = \frac{U_{DC}}{U_{AC\_RMS}} \quad (13)$$

where U_{AC_RMS} is the root-mean-square (RMS) value of AC voltage. For the sake of clarity, the simulated results are divided into two groups. One contains simulated results under 50 Hz 9 kV(RMS) pure AC stresses, under 9 kV pure DC stress, and under 50 Hz 9 kV(RMS)combined AC and DC stress with DC offset's ratio of 0.2, 0.5, and 1, aiming to present the effects of the DC component percentage within the combined stresses. The applied fields used in this group in shown in Fig.4, where the pure AC and combined stresses own an overshoot over the 9 kV RMS value, and the combined stresses with higher DC offset's ratio have more above zero values over time.

In the first group, the chosen field frequency is 50 Hz, which is utilised to reflect the common situation in high voltage power systems. And the selected ratio values are 0, 0.2, 0.5, 1, ∞, aiming to present a complete evolution of the DC offset's ratio influences within the combined stresses on the charge dynamic with in insulations.

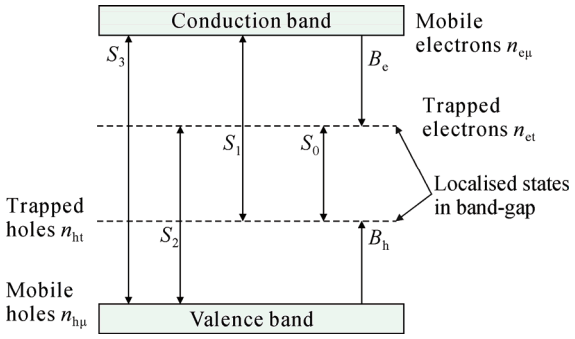

Fig.3 Trapping and recombination of bipolar charge carriers

Table 1 Parameters for space charge under combined AC and DC simulation

Parameter		Value
Sample thickness/μm		180
Barrier height for injection/eV	w_{et}(electrons)	1.18
	w_{ht}(holes)	1.16
Low field mobility μ_0/($m^2 \cdot V^{-1} \cdot s^{-1}$)		4.5×10^{-16}
Power law's index of mobility n/($m^2 \cdot V^{-1} \cdot s^{-1}$)		1.165
Trap density/($C \cdot m^{-3}$)	N_{0et}(electrons)	100
	N_{0ht}(holes)	10
Trapping coefficients/ s^{-1}	B_e(electrons)	7×10^{-3}
	B_h(holes)	7×10^{-5}
Recombination coefficients/($m^3 \cdot C^{-1} \cdot s^{-1}$)	S_0 trapped electron-trapped hole	4×10^{-3}
	S_1 mobile electron-trapped hole	4×10^{-3}
	S_2 trapped electron-mobile hole	4×10^{-3}
	S_3 mobile electron-mobile hole	0

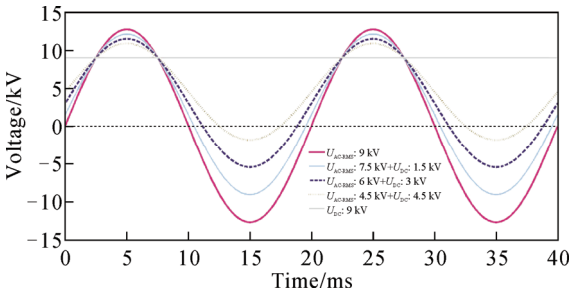

Fig.4 First two cycles of applied combined stress with different DC offsets

The other group contains results under 0.05 Hz, 0.5 Hz, 5 Hz and 50 Hz (power frequency), 4.5 kV (RMS) AC with 4.5 kV DC voltages, in order to demonstrate the influence of the AC component's frequency within the applied stresses. This selection of the analysed frequencies followed the paper of Tanaka *et al*. which investigated the frequency dependence of charge density under AC stress[16]. In the paper they reported that the amount of charge within insulation under AC stress shows a sharp decrease only when the frequency is increased within the range between 10^{-3} Hz and 10^{-2} Hz, and only slight decreases were observed outside the abovementioned frequency range. In this way, in this group, the selected external electric fields include 0.05 Hz and 0.5 Hz, to clearly show the degree of variation of impacts of frequencies of AC component on charge dynamics. And the DC offset's ratio chosen in this group is fixed to 1, aiming to show the frequency influence of a balanced combined stresses, where AC and DC component sharing the same RMS value, on the charge dynamic within sample.

The simulated charge distribution curve under 50 Hz pure AC fields is shown in Fig.5. The charge dynamics under 50 Hz combined AC and DC with DC offset's ratio of 0.2, 0.5 and 1 are respectively presented in Fig.4 to Fig.8. Fig.9 shows charge profiles under pure DC voltage. Charge profiles under 0.5 Hz combined AC and DC with DC offset's ratio 1 is illustrated in Fig.10.

Fig.5 gives the charge distribution sranging from 30s to 60 minutes under 50 Hz pure AC conditions, and the trends of charge development are marked using the arrows. From the graph, it is clearly the positive charge accumulation takes place near both electrodes and transport into the bulk area as a peak. The front edges of positive charge peaks are changing one from the ground side starts at 0.011 mm, at 30 s, and to 0.028 mm at 60 min while the other from the opposite electrode from 0.171 mm at 30 s and to 0.150 mm at 60 min. This is because more holes are injected at both electrodes due to holes' lower injection barrier, during each half cycle, and slower transport owing to its lower mobility within the sample. In this way, positive charge will be accumulated near the two electrodes. However, the electrons, although in a small amount, can move further into the bulk area. The front edges of negative charge peaks move one from 0.033 mm at 30 s to 0.078 mm at 60 min from the ground and the other from 0.147 mm at 30 s, to 0.087 mm at 60 min, from the opposite electrode. With time, both accumulated peaks become larger, and maximum charge densities of both charge carriers increased. The maximum charge density value changes from 3.926 C/m^3 to 4.414 C/m^3 and from 6.270 C/m^3 to 8.570 C/m^3 for holes, while from –0.106 C/m^3 to –0.247 C/m^3 and from –0.147 C/m^3 to –0.527 C/m^3 for electrons.

Fig.6 shows charge distributions under 50 Hz combined AC and DC stress with DC offset's ratio 0.2. Unlike Fig.5, negative charge and positive charge can only be observed from one electrode, due to the DC offset's effects. A negative charge peak can be observed near the ground side and this peak increases its maximum value along with time, from –4.326 C/m^3 to –38.660 C/m^3. The position of the maximum value

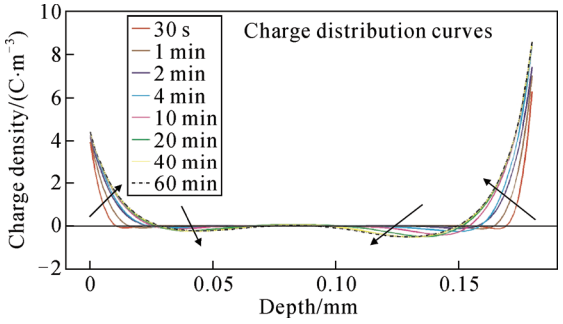

Fig.5 Charge distribution under 9 kV (RMS) 50 Hz purely AC stress

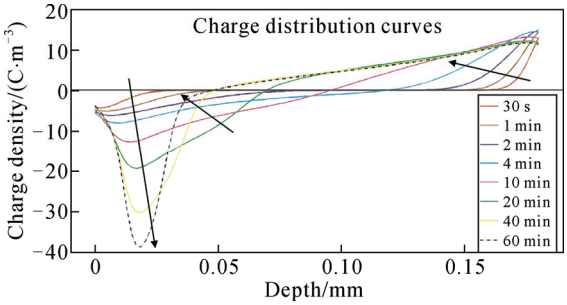

Fig.6 Charge distribution under 7.5 kV (RMS) 50 Hz AC +1.5 kV DC stress

of negative peak occurs at around 0.002 mm at 30 s and at around 0.017 mm at 60 min. The reason is that a larger amount of charges can remain and transport into the bulk of the insulator under the combined AC and DC condition. The negative charges injected from the ground, move quickly to meet the front edge of the positive charge peak, due to the DC offset's effects. However the negative charges near the ground sides can be neutralised by the newly injected positive charges, making the negative charge peak distorts sharply with time. As for positive charge under this condition, they move faster and further than those under pure AC condition from 0.156 mm at 30 s to 0.048 mm at 60 min. This phenomenon is caused by a large amount of charge injections under the applied field.

Fig.7 shows the simulated charge distribution results under combined stress (AC at 50 Hz) with one third DC voltage component's contributions. Similar to Fig.6, negative and positive charge can only be observed from one side. But negative charge density peak value is reduced, especially for the cases after 20min, comparing with Fig.6. It can be seen that the maximum value of negative peak at 40 min and 60 min in Fig.6 is around –30 C/m^3 and –40 C/m^3. However, in the case of Fig.7 it is around –20 C/m^3. The positions where the maximum values occur in Fig.7 are all near the ground side. This is because within this applied field, the larger DC component lifts the alteration point of field up to a higher value. This leads to the positive charges injected from the ground side, occurring when the applied filed is negative, are not strong enough to significant effect the movement of the injected negative charges. In this way, the negative charge peak will be dominated by the positive charge packet from the other side, moving towards the ground electrode, in comparison with those in Fig.5 and Fig.6. When the negative peak is near the ground, it will be consistently neutralised by the newly injected holes, resulting in the reduction of negative peak values.

Under this combined condition, the positive charges transport faster, in comparison with that in Fig.6 due to the longer time of positive polarity of the applied field, causing a higher degree of internal field distortion.

Fig.8 presents charge distributions under 50 Hz combined AC and DC stress with DC offset's ratio 1. The overall trend and shape are similar to Fig.7, but the positive charge packet moves faster, from 0.137 mm at 30 s to 0.028 mm at 60 min. Besides, the dynamic of charge transport ends quicker in Fig.8 and no significant change can be observed from the charge profiles after 10 min (For the time for this equilibrium is 20 min in Fig.7; in Fig.6 the equilibrium has not been reached within the simulated 60 min).

Fig.9 illustrates the simulation results under 9 kV DC using the same parameter settings. It is presented to provide comparison. A clear positive charge packet

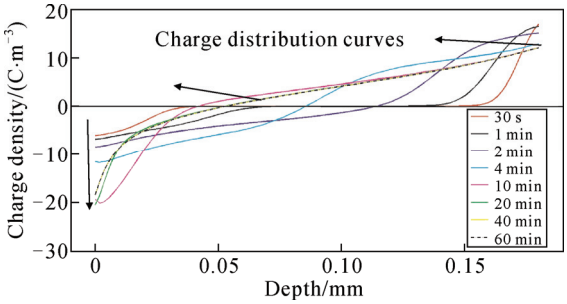

Fig.7 Charge distribution under 6 kV (RMS) 50 Hz AC +3 kV DC stress

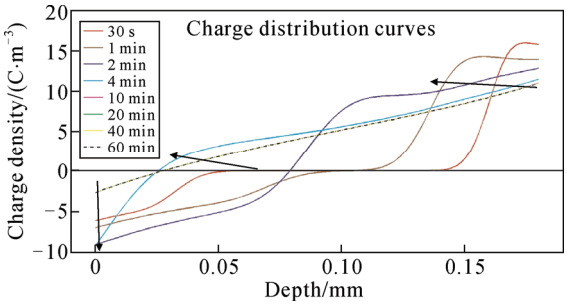

Fig.8 Charge distribution under 4.5 kV (RMS) 50 Hz AC +4.5 kV DC stress

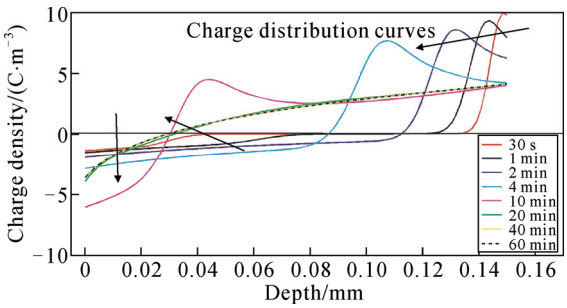

Fig.9 Charge distribution under 9 kV DC stress

develops initially and becomes broader (diffused) when moving across the sample.

From Fig.5 to Fig.9, it is noticeable that the charge distribution curves from pure AC electric field are significantly different from those under the combined electric stresses. Negative charge accumulation can only be observed near the ground electrode for charge distribution curves under the combined electric stresses. The shape of the charge distribution curves is much more like the distribution curve under pure DC conditions when the DC offset's ratio is relatively high (≥0.5).

Furthermore, the magnitude of the injected charge density under combined stresses is larger than that under pure AC stress when comparing Fig.5 with Fig.6 to Fig.8. This is because the DC offsets cause an unsymmetrical time of positive and negative charge injections, as shown in Fig.4, which will enhance the net charge injections. A large amount of charges will be injected at the above 9 kV (RMS value of the applied fields) time period since the Schottky injection indicates the injected charge amount has an exponential relationship with the electric field.

The frequency influence of the AC component of the combined electric field has been investigated. Fig.10 demonstrates a typical result of charge distribution under combined stress when the AC component frequency is relatively low. The accumulated positive charges move like a packet towards the opposite electrode with time, similar to the positive charge movements under DC condition (Fig.9), due to the influence of 50% DC component within the applied field. However the peak values of both accumulated holes and electrons under the combined condition are larger than those under DC condition. This is because the maximum magnitude of the applied combined field is larger than that of DC field owing to the AC component, causing a larger amount of charge injections. Hardly can the differences between Fig.10 and Fig.8 (same voltage ratio for AC and DC component while under a higher AC component's frequency of 50 Hz) be distinguished, due to frequency's limited

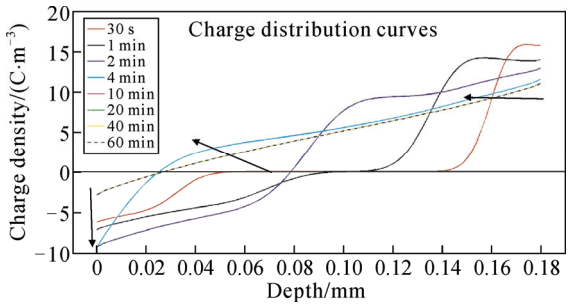

Fig.10 Charge distribution under 4.5 kV (RMS) 0.5 Hz AC +4.5 kV DC stress

effects on the charge distribution simulation under combined AC and DC stresses. In this way, the integration is applied to get the charge amount within the sample alteration along with time. Using this method, the influences of both DC offset's ratio and AC component's frequency on the charge dynamic within the sample can both be distinguished and compared. Specific information is shown in the following section.

3 Analysis and Discussion

In this section, the influences of both DC component percentage and frequency of AC component are analysed. Part A concerns with charge dynamics within polyethylene under various DC component percentages; while part B deal with the impact of frequency on charge accumulation in the material.

In order to illustrate the overall charge accumulation information within the insulation and clearly demonstrate the factors' influences, the charge distribution over spatial coordinate is integrated to obtain the total charge amount, which has been used to analyse and discuss the simulation results. The integration of charge used is shown in Equation (14).

$$C_{\mathrm{T}}(t)=\int_0^d \rho(x,t)\mathrm{d}x \tag{14}$$

where C_{T} is the total charge amount as a function of time; d is the sample thickness and ρ is the charge density, a function of time and spatial coordinate.

3.1 Dynamics of space charge under different DC offset's ratio

In this part, the integrations of simulated results under 50 Hz combined AC and DC stresses with various DC offset's ratio are presented, aiming to

demonstrate the offset's ratio effects on the charge dynamic within the insulation. Integral net charge, positive charge and negative charge amount are illustrated in Fig.11 to Fig.13

Fig.11 presents the net charges within the sample under combined stresses within different DC offsets. The overall trend for the curves shows a dynamic period followed by a saturation period. And for the majority cases, the charge amount curves reach steady states at around 20 minutes. There is an exception for the case under combined AC and DC fields with DC ratio 1, here the dynamic ends sharply within initial 10 minutes. The mobility of both carriers increases when the electric stress intensifies, which causes the shortened dynamic periods. The saturation net charge amounts for the five conditions are divergent. The maximum saturation amount occurs at DC offset's ratio 1, while the minimum happens at offset's ratio 0.2. When the DC offset's ratio is higher than 0.5, the steady state net charge amount is higher than amounts accumulated under pure AC and DC conditions. However when DC offset's ratio is small, like 0.2, the steady state net charge amount can even be smaller than the amount gathered under pure AC condition. To uncover the reality behind this outcome, the total positive charge amount and negative charge amount and their variation with time are also analysed.

Fig.12 and Fig.13 present the specific information of the integrated positive and negative charge. It can be observed that, the magnitude of both positive and negative is similar, causing smaller net charges amounts presented in Fig.11. For positive charges, the charge amount for pure DC is higher than the amount for pure AC while lower than those for combined conditions. The charge amount obtained for the combined conditions increases along with DC offset ratio.

Nevertheless, the case for negative charge is much more complicated. The integrated charge amount with a lower DC offset's ratio is approximately the same for negative charge, and the same goes for the amount gained under pure AC and DC. But the negative charge amount will reach a relatively high steady state, comparable to the positive charge

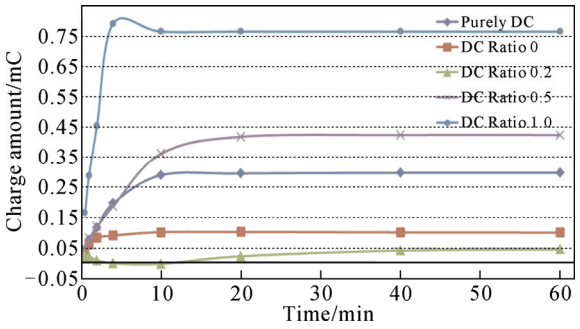

Fig.11 Integral net charge's trend over time under various ratios

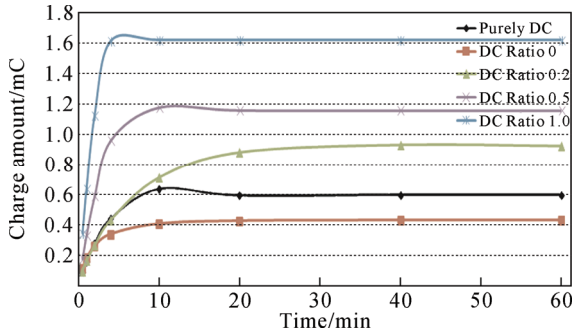

Fig.12 Integral positive charge's trend over time under various ratios

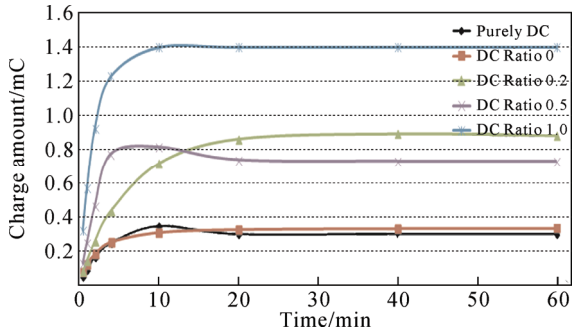

Fig.13 Integral negative charge's trend over time under various ratios

amount under the same condition when DC offset's ratio is one. This is owing to the effect of holes' lower injection barrier. It is expected that the injected positive charges are excessive comparing with the negative charges. Consequently, the positive peaks in the distribution curve under pure AC fields dominate the net charge amount transient and saturating process and strongly affect the dynamic of negative charges. Under combined conditions with relatively low DC offsets, where the injection of electrons is not strong enough to

compensate the influence of positive charge, the amount of electrons will show complex relationship with DC offsets, unlike for holes, always positive correlation.

Overall, the DC offset's ratio within the applied combined AC and DC stresses, mainly influences the positive charge transport within the insulation to affect the charge distribution within the context of selected parameters for the simulation model. The higher the DC offset's ratio, the larger positive charge amount. Higher DC offset's ratio can also help to shorten the charge dynamic period within sample to reach a steady state.

3.2 Dynamics of space charge under different AC component's frequency

The space charge distribution profiles are simulated by the bipolar model, however, the differences among the curves under various frequencies are difficult to distinguish (comparing Fig.8 with Fig.10), due to the limited impact caused by the variable frequencies. Therefore, in this part, the charge is integrated using Equation (14) to demonstrate the influence of AC component within the applied combined stresses.

Fig.14 to Fig.16 show the integrated values of net charge, positive charge and negative charge over 60 minutes. Because the differences among the results under high frequencies are too small to distinguish, the high frequency part is zoomed in as shown on the top right corners of Fig.14 to Fig.16.

Fig.14 shows the integral net charge amount within the insulation under pure DC stress, under combined AC and DC stresses with frequency ranging from 0.05 Hz to 50 Hz. It can be clearly observed from the graph that the amounts of net charge under the combined AC and DC stresses are significantly larger than that under the DC conditions. And the net charge amount decreases with increasing frequency, and this phenomenon becomes insignificant when the applied field frequency is higher than 0.5 Hz. It seems that there exists a frequency range within which charge accumulation in the material drops rapidly under combined AC and DC conditions. This observation is consistent with the experimental results under pure AC

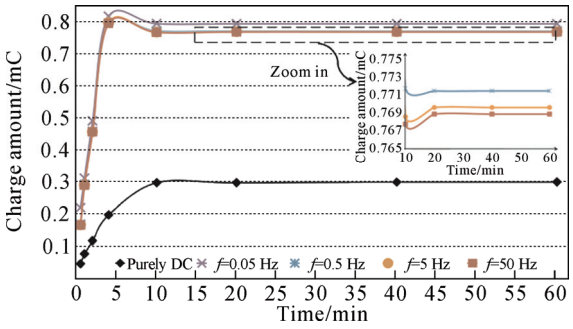

Fig.14 Integral net charge's trend over time under various frequencies

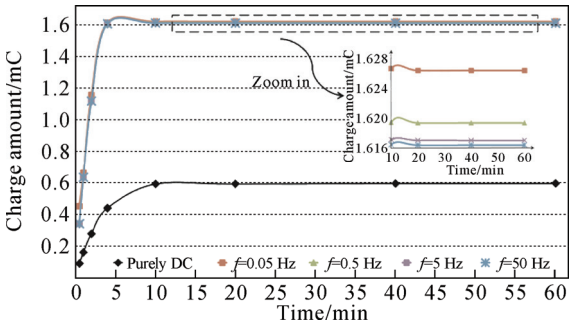

Fig.15 Integral total positive charge's trend over time under various frequencies

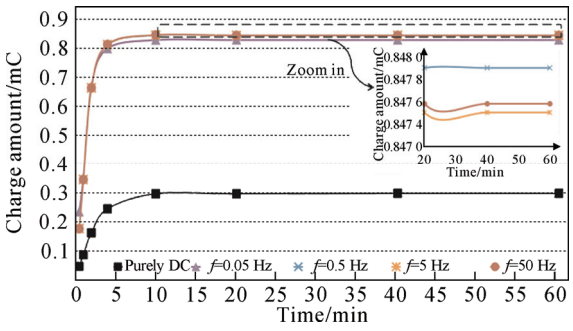

Fig.16 Integral total negative charge's trend over time under various frequencies

conditions[6], which is also consistent with the frequency range found by Tanaka *et al*. who reported that the charge within insulation's amount decreased sharply when the applied fields' frequency changed from 10^{-3} to 10^{-2}[16].

Besides, it can also be observed that the amount of net charges within the insulation under combined stress is positive. In the present model it is assumed that holes are easier to be injected into the insulation (lower injection barrier) comparing with electrons.

Therefore, holes show dominance in charge accumulation dynamics.

Furthermore, as shown in Fig.14, the charge amount varies dramatically within the first 20 minutes. And a small increase in the transient time can be observed, along with frequency increasing. But the transient time is reduced greatly under the combined stresses in comparison with that under pure DC conditions. And this is because positive charges are moving faster under the applied combined AC and DC conditions, comparing with under pure DC conditions, due to the holes' mobility field-dependent effects (Fig.2).

Fig.15 and Fig.16 are the integrated results of positive charge and negative charge amounts. Similar to the net charge amount curve, the total positive charge saturates at around 20 minutes. The higher the frequency is, the longer it takes to reach the steady state. As a comparison, the transient time for electrons under higher frequency (≥5 Hz) is generally longer, around 30~40 minutes. This indicates the frequency of the applied combined stress has stronger influence on the negative charge movements due to the larger variable range of the mobility of the negative charges than positive charges.

The total positive charge amount and total negative charge amount under combined conditions are also larger than those under pure DC conditions. And the overall accumulated positive charge amount is larger than negative amount.

Furthermore, with the frequency increasing, the saturated amount of holes decreases. In contrast, this is not the case for electrons. The minimum amount of the saturated electrons occurs at the frequency of 0.05 Hz instead of 50 Hz. But because the positive charge amount is larger than the negative charge amount, the net charge amount decreases with the increase of frequency.

In summary, the simulated results show net charge amount decreases with increasing of AC component's frequency within the applied fields. Sharp change occurs within the frequency range of 10^{-3} to 10^{-2}. The frequency of the AC component affects the overall charge dynamics, mainly via its influence on the positive charge injection and transport processes

4 Conclusions

Space charge within LDPE under combined AC and DC stress has been simulated using the bipolar charge transport model in this paper.

1) The accumulation of space charge under AC stress can be weakened by the frequent reversal of the applied field while the addition of the DC component can neutralise this effects, and even enhance the charge gathering when the component ratio exceeds a certain value. Besides, DC offsets within the combined stress can also distort the charge distribution further, assisting the charge near the surface area transport through into the bulk of the insulation.

2) The results also show that the increasing frequency of AC component within the applied combined stress can reduce the amount of the accumulated charges and the reduction becomes insignificant when the frequency is higher than 0.5 Hz. Besides the frequency of the AC component within the applied electric fields can increase the time for the system to reach the steady state. This effect is also relatively weak when the frequency is high.

3) Furthermore the DC offset's ratio and AC component's frequency within the combined AC and DC applied fields affect charge dynamics within the insulation via their influence on the positive charge.

4) All these above show that, unlike under AC conditions, the space charge under complex electric stresses should be paid more attention as they may occur in practical applications. Especially, experimental work needs to be done to validate/guide the simulation work. Modification on the model can be made to match practical situations, if sufficient measurement results become available. The correct modelling will assist our understanding of physical processes of charge dynamics within the insulating materials.

References

[1] Li Y, Takada T. Progress in space charge measurement of solid insulating materials in Japan[J]. IEEE Electrical Insulation Magazine, 1994,

10(5): 16-28.

[2] Fleming R J. Space charge in polymers, particularly polyethylene[J]. Brazilian Journal of Physics, 1999, 29(2): 280-294.

[3] Alison J M, Hill R M. A model for bipolar charge transport, trapping and recombination in degassed crosslinked polyethene[J]. Journal of Physics D: Applied Physics, 1994, 27(6): 1291-1299.

[4] Roy S L, Segur P, Teyssedre G, *et al*. Description of bipolar charge transport in polyethylene using a fluid model with a constant mobility: model prediction[J]. Journal of Physics D: Applied Physics, 2004, 37(2): 298-305.

[5] Belgaroui E, Boukhris I, Kallel A, *et al*. A new numerical model applied to bipolar charge transport, trapping and recombination under low and high DC voltages[J]. Journal of Physics D: Applied Physics, 2007, 40(21): 6760-6767.

[6] See A, Fothergill J C, Dissado L A, *et al*. Measurement of space-charge distributions in solid insulators under rapidly varying voltage using the high-voltage, high-speed pulsed electro-acoustic (PEA) apparatus[J]. Measurement Science & Technology, 2001, 12(8): 1227-1234.

[7] Chen G, Fu M, Liu X Z, *et al*. AC aging and space-charge characteristics in low-density polyethylene polymeric insulation[J]. Journal of Applied Physics, 2005, 97(8): 083713.

[8] Alison J M, Hill R M. A model for bipolar charge transport in insulators[C]// 1995 IEEE 5th International Conference o Conduction and Breakdown in Solid Dielectrics. Leicester, UK: IEEE, 1995: 319-323.

[9] Roy S L, Teyssedre G, Laurent C, *et al*. Numerical modeling of space charge and electroluminescence in polyethylene under DC field[C]// 2002 Annual Report Conference on Electrical Insulation and Dielectric Phenomena. Cancun, Mexico: IEEE, 2002: 172-175.

[10] Roy S L, Teyssedre G, Laurent C, *et al*. Description of charge transport in polyethylene using a fluid model with a constant mobility: fitting model and experiments[J]. Journal of Physics D: Applied Physics, 2006, 39(7): 1427-1436.

[11] Zhao J, Xu Z, Chen G, *et al*. Numeric description of space charge in polyethylene under AC electric fields[J]. Journal of Applied Physics, 2010, 108(12): 124107.

[12] Chen G, Zhao J W. Observation of negative differential mobility and charge packet in polyethylene[J]. Journal of Physics D: Applied Physics, 2011, 44(21): 212001.

[13] Zhao J, Xu Z, Chen G, *et al*. Effect of field-dependent mobility on current density and dynamics of space charge in polyethylene[C]// 2009 Annual Report on Conference on Electrical Insulation and Dielectric Phenomena. Virginia Beach, USA: IEEE, 2009: 120-123.

[14] Chen G, Zhao J, Li S, *et al*. Origin of thickness dependent DC electrical breakdown in dielectrics[J]. Applied Physics Letters, 2012, 100(22): 222904.

[15] Zhao J, Chen G, Lewin P L. Investigation into the formation of charge packets in polyethylene: experiment and simulation[J]. Journal of Applied Physics, 2012, 112(3): 034116.

[16] Tanaka T, Ito T, Tanaka Y, *et al*. Frequency dependence of interfacial space charge formed in laminated dielectrics under AC voltage application conditions[C]// 2000 Annual Report Conference on Electrical Insulation and Dielectric Phenomena. Victoria, Canada: IEEE, 2000: 796-799.

Churui Zhou was born in China in 1991. She received her B.Eng. degree (2013) in Electrical Engineering from Huazhong University of Science and Technology, China and B.Eng. degree in Electrical Engineering (2013) from University of Birmingham, UK. Since 2013, she has been a Ph.D. student in the University of Southampton, UK. Her main research interest is experimental and numerical modelling of space charge in polyethylene under complex electric fields.

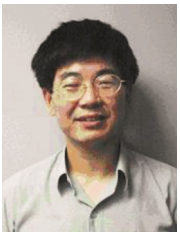

George Chen(SM'11) was born in China in 1961. He received the B.Eng. (1983) and M.Sc. (1986) degrees in electrical engineering from Xi'an Jiaotong University, China. After he obtained the Ph.D. degree (1990) from the University of Strathclyde, UK, on the work of permanent changes in electrical properties of irradiated low-density polyethylene, he joined the University of Southampton as postdoctoral research fellow and became a senior research fellow subsequently. In 1997 he was appointed as a research lecturer and promoted to a Reader in 2002. He is now the professor of high voltage engineering at the University of Southampton and a visiting professor of Xi'an Jiaotong University. Over the years, he has developed a wide range of interests in high voltage engineering and electrical properties of materials and published over 300 papers. He is active in the HVDC systems and involved with technical working groups in both IEEE and CIGRE.

Received date 2014-11-25
Editor XIAO Zheng